

First infrared spectroscopic characterization of the disilyl (Si_2H_5) and d5-disilyl (Si_2D_5) radicals in low temperature silane matrices

David Sillars^a, Chris J. Bennett^a, Yoshihiro Osamura^b, Ralf I. Kaiser^{a,*}

^a Department of Chemistry, University of Hawai'i at Manoa, Honolulu, HI 96822, USA

^b Department of Chemistry, Rikkyo University, 3-34-1 Nishi-ikebukuro, Tokyo 171-8501, Japan

Received 7 January 2004; accepted 25 May 2004

Available online 27 July 2004

Abstract

The disilyl, $\text{Si}_2\text{H}_5(\text{X}^2\text{A}')$, and the d5-disilyl, $\text{Si}_2\text{D}_5(\text{X}^2\text{A}')$, radicals were observed for the first time via infrared spectroscopy in low temperature silane matrices at 10 K upon an irradiation of the silane matrices with mono energetic electrons. We were able to observe absorptions of the umbrella modes at 843 (silane matrix) and at 621 cm^{-1} (d4-silane matrix). Accounting for a scaling factor of 0.97, ab initio DFT data predict that the most intense absorption of the disilyl radical should be observable at 843 ($\text{Si}_2\text{H}_5(\text{X}^2\text{A}')$) and 621 cm^{-1} ($\text{Si}_2\text{D}_5(\text{X}^2\text{A}')$). These computed data are in excellent agreement with our observations. The blue shift of the Si–H and Si–D modes from 820 (Si_2H_6) to 843 cm^{-1} (Si_2H_5) and 606 (Si_2D_6) to 621 cm^{-1} (Si_2D_5) goes hand in hand with a change from a sp^3 to an sp^2 hybridized silicon atom. This knowledge of the infrared absorption features might help to follow the chemical evolution of silicon CVD process not only via mass spectrometry, but also through time resolved infrared spectroscopy monitoring the most intense umbrella mode of the disilyl species. Further, the infrared frequencies provide vital guidance to search for hitherto undetected silicon-bearing species in the circumstellar envelope of the carbon star IRC+10216.

© 2004 Elsevier B.V. All rights reserved.

1. Introduction

An understanding of the spectroscopic properties and energetics of simple silicon bearing species such as the SiH_x ($x=1-3$) and Si_2H_x ($x=1-5$) series is of crucial importance to untangle the elementary chemical reactions involved in silicon chemical vapor deposition (CVD) processes and in circumstellar envelopes of dying carbon stars. Together with reactive plasmas and plasma etching processes [1–4], CVD techniques are of wide technological interest to produce silicon bearing nano particles and amorphous silicon films (a-Si:H) via microelectronic engineering. Here, silane (SiH_4) and disilane (Si_2H_6) are often the key material for the production of amorphous silicon films. However, to optimize and even to control

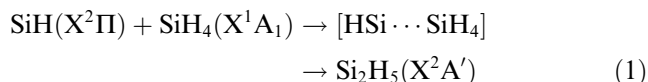
the nucleation processes, the underlying chemical mechanisms have to be understood in depth. Complex reaction networks which actually model CVD processes [5,6], require crucial input parameters such as rate constants of the reactions involved, reaction products, and their thermochemical data [7,8]. Since not only neutral species such as the silyl radical but anions have been observed as rate-limiting reagents as well, it is also important to provide detailed data on the electron affinities of the neutral species [9,10].

The properties and formation routes of the disilyl radical, $\text{Si}_2\text{H}_5(\text{X}^2\text{A}')$ have received particular attention since this species has been identified to contribute significantly to the growth of silicon bearing nanostructures in plasma- and photo-initiated silane CVD [11,12]. A recent computational study identified the disilyl radical also as a reactive intermediate. Here, $\text{Si}_2\text{H}_5(\text{X}^2\text{A}')$ was computed to be formed via an initial van-der-Waals complex of a silylydyne radical, $\text{SiH}(\text{X}^2\Pi)$, with a SiH_4 molecule

* Corresponding author.

E-mail address: kaiser@gold.chem.hawaii.edu (R.I. Kaiser).

followed by insertion of the SiH species into the silicon–hydrogen bond via a barrier of 15 kJ mol^{-1} . The reaction exoergicities to form the initial complex and the disilyl radical were calculated to be 24 and 163 kJ mol^{-1} , respectively [13]. An alternative formation route proceeds via an excited triplet state of disilane, $\text{Si}_2\text{H}_6(a^3A_{2u})$. Here, an excitation from the $^1A_{1g}$ ground state requires 661 kJ mol^{-1} ; this is followed either by a simple silicon–silicon or silicon–hydrogen bond rupture, reactions (2) and (3). The overall reaction endoergicities for (2) and (3) were found to be 211 and 288 kJ mol^{-1} , respectively [14].

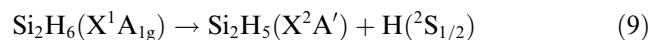
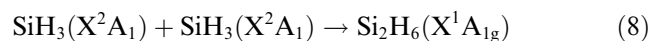
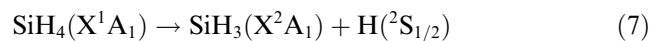
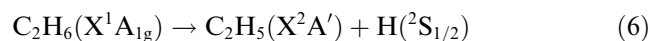
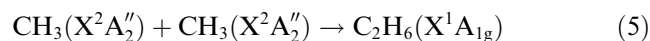
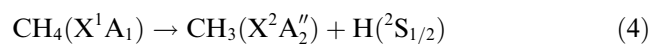


To validate these studies, it is important to compare the calculations with actual CVD experiments. Very recently, the surface reaction probabilities of the disilyl radical, $\text{Si}_2\text{H}_5(X^2A')$, were probed via time resolved threshold ionization mass spectrometry [2]. The disilyl radical has been also prepared via the gas phase reaction of fluorine atoms with disilane and detected through photo ionization mass spectrometry; the ionization potential of disilyl was determined to be 7.6 eV [15] giving an enthalpy of formation of the disilyl species of 248–265 kJ mol^{-1} . However, despite the importance of the disilyl radical as a rate limiting growth species of a-Si:H films in CVD processes of silane and disilane reactors, the vibration levels of the disilyl radical have not been investigated experimentally. Here, a detailed knowledge of the infrared absorption features might help to follow the chemical evolution of silicon CVD process not only via mass spectrometry, but also through time resolved infrared spectroscopy.

These studies are not only relevant to better understand CVD processes, but might also assist an identification of silicon-bearing molecules in the circumstellar envelopes of dying carbon stars such as IRC+10216. About 15% of the observed interstellar molecules contain silicon ranging from simple diatomics (SiC, SiN, SiO, SiS), via triatomics (SiCN) and a silicon-terminated cummulene (CCCCSi) to two cyclic species (SiC_2 , SiC_3) [16,17]. Here, the silane molecule – a potential precursor to more complex organo silicon molecules – has also been detected in the outflow of carbon stars [18].

In this paper, we present for the very first time a combined experimental and theoretical study on the disilyl radical and elucidate the position of the most intense, hitherto elusive infrared absorption frequencies of this species and of the perdeuterated counterpart in low temperature silane matrices; a complete description of the SiH_x and Si_2H_x potential energy surfaces are given in

a forthcoming publication. It has been demonstrated earlier, that an interaction of energetic electrons can cleave a carbon–hydrogen bond in a methane molecule to form atomic hydrogen and a methyl radical at 10 K, reaction (4). Two neighboring methyl radicals were found to recombine forming an ethane molecule (5) [19]. Upon further irradiation with electrons, the ethane molecule decomposes to a hydrogen atom plus an ethyl radical, Eq. (6). Here, we expand this protocol and attempt to synthesize the disilyl radical via a homologous reaction sequence, reactions (7)–(9).



2. Experimental

The experiments were carried out in a contamination-free ultrahigh vacuum (UHV) chamber; the top view of this machine is shown in Fig. 1. This vessel consists of a 15 l cylindrical stainless steel chamber of 250 mm diameter and 300 mm height which can be evacuated down to 2×10^{-10} torr by a magnetically suspended turbopump backed by an oil-free scroll pump. A rotatable, two stage closed cycle helium refrigerator is attached to the lid of the machine and holds a polished silver mono crystal. This crystal is cooled to $10.2 \pm 0.3 \text{ K}$ and serves as a substrate for the ice condensate. The silane and d4-silane ice condensation is assisted by a precision leak valve. The latter is connected to a gas reservoir and rests on a linear transfer mechanism; during the actual gas condensation, the deposition system can be moved 5 mm in front of the silver target. This setup guarantees a reproducible thickness of the silane frosts at 10 K. The silane ices were prepared at 10 K by depositing silane (99.99%) and d4-silane (99.99%) at pressures of 6×10^{-8} torr for 30 min onto the cooled silver crystal. Fig. 2 depicts a typical infrared spectrum of the silane frost at 10 K; the absorptions are compiled in Table 1.

To determine the ice thickness quantitatively, we integrated the infrared absorption features at 2163 and 876 cm^{-1} and calculated the ice thickness via the Lambert–Beers relationship [20]. Considering the integrated absorption coefficients of these fundamentals, i.e., 2.5

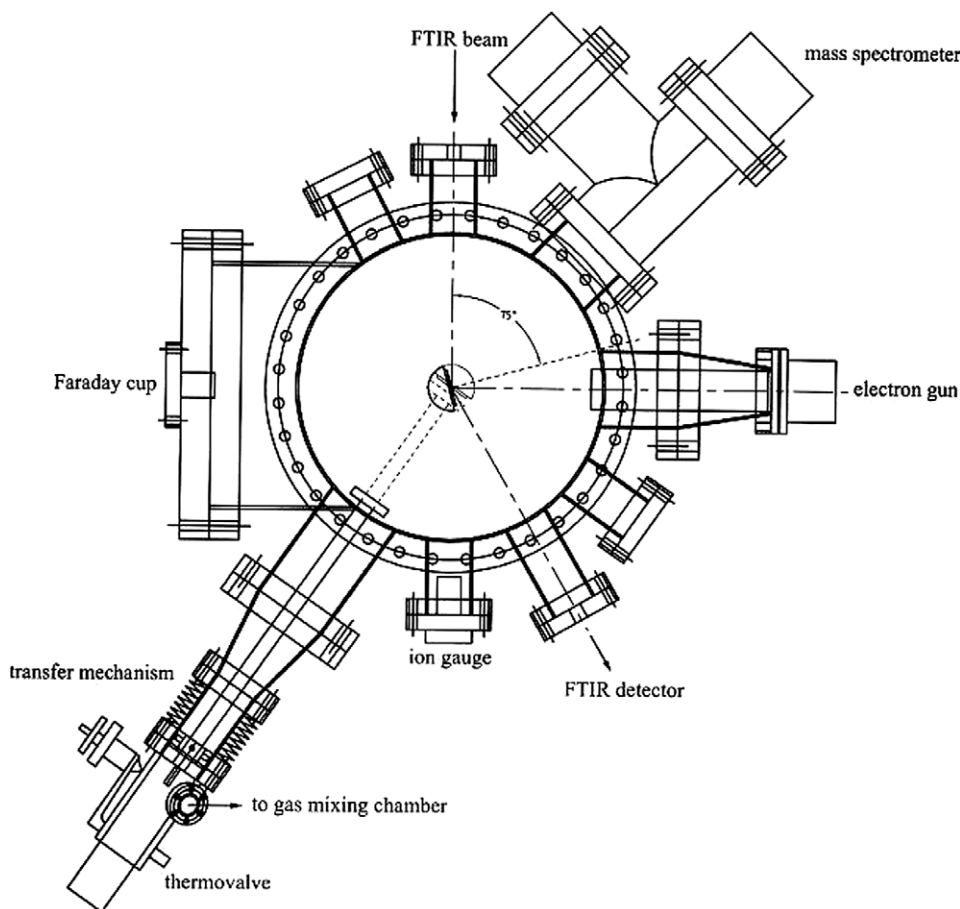


Fig. 1. Top view of the experimental setup.

and 2.0×10^{-17} cm, and a density of the silane ice of 0.77 ± 0.03 g cm $^{-3}$ [21], this translates into an optical thickness of 0.21 ± 0.01 μ m silane.

We like to comment briefly on the modification of the condensed silane samples. In the gas phase, the T_d symmetric silane molecule has four vibrational modes of F_2 (ν_3 ; 2191 cm $^{-1}$), F_2 (ν_4 ; 914 cm $^{-1}$), E (ν_2 ; 975 cm $^{-1}$), and A_1 symmetry (ν_1 ; 2187 cm $^{-1}$). Only the asymmetrical stretching (ν_3 , F_2) and the bending modes (ν_4 , F_2) are infrared active. The inactive symmetric stretching mode ν_1 appears in Raman spectra at lower wavelength close to ν_3 ; the doubly degenerate bending mode ν_2 is also infrared inactive in the gas phase. In the solid state, silane exists in two tetragonal phases: orientationally disordered $\text{SiH}_4(\text{I})$ ($T > 63.45$ K) and a birefringent phase $\text{SiH}_4(\text{II})$ [22]. In the high temperature phase, molecules undergo fast rotation, whereas in phase II the silane molecules are oriented at sites of symmetry C_1 . The ν_3 and ν_4 are observable in phase I and II, whereas the ν_2 bending mode becomes infrared active only in phase II due to the lower site symmetry of the silane molecules [23]. Overtone and combination bands are also observable such as at 4354 ($2\nu_3$) and 4283 cm $^{-1}$ ($\nu_1 + \nu_3$); in phase I, both absorptions are very broad; as the temperature decreases and phase II becomes the thermodynamically

more stable ones, the vibrational bands exhibit well-resolved fine structures. Note that a splitting is observed also for the ν_3 and ν_4 fundamentals at $T < 63.45$ K due to the lower site symmetry of the silane molecules in $\text{SiH}_4(\text{II})$. We would like to stress that upon the transition from the gas to the solid phase, lattice modes appear in the infrared spectrum of solid silane, too. Here, three lattice vibrations have been detected in previous studies at 160–104 cm $^{-1}$ (γ ; librational), 89–77 cm $^{-1}$ (β ; librational), and at 33–27 cm $^{-1}$ (α ; translational) [24]. In phase II, distinct bands are observable at $\nu_3 + \alpha$, $\nu_3 + \beta$, and $\nu_3 + \gamma$; as the temperature rises, these absorptions merge to a broad bump centered around 2290 cm $^{-1}$. We can compare these literature data with our infrared spectrum of the silane sample (Fig. 2 and Table 1). The absorptions suggest that the frozen high temperature modifications of $\text{SiH}_4(\text{I})$ and $\text{SiD}_4(\text{I})$ dominate the constitution of the sample. However, the presence of the ν_2 peak, which is infrared inactive in crystalline $\text{SiH}_4(\text{I})$, suggests that the sample is partially disordered, possibly amorphous. We would like to stress that $\text{SiH}_4(\text{II})$ can be excluded because we do not observe any fine structure in ν_3 and ν_4 .

These ices were irradiated at 10 K with 5 keV electrons generated in an electron gun at beam currents of

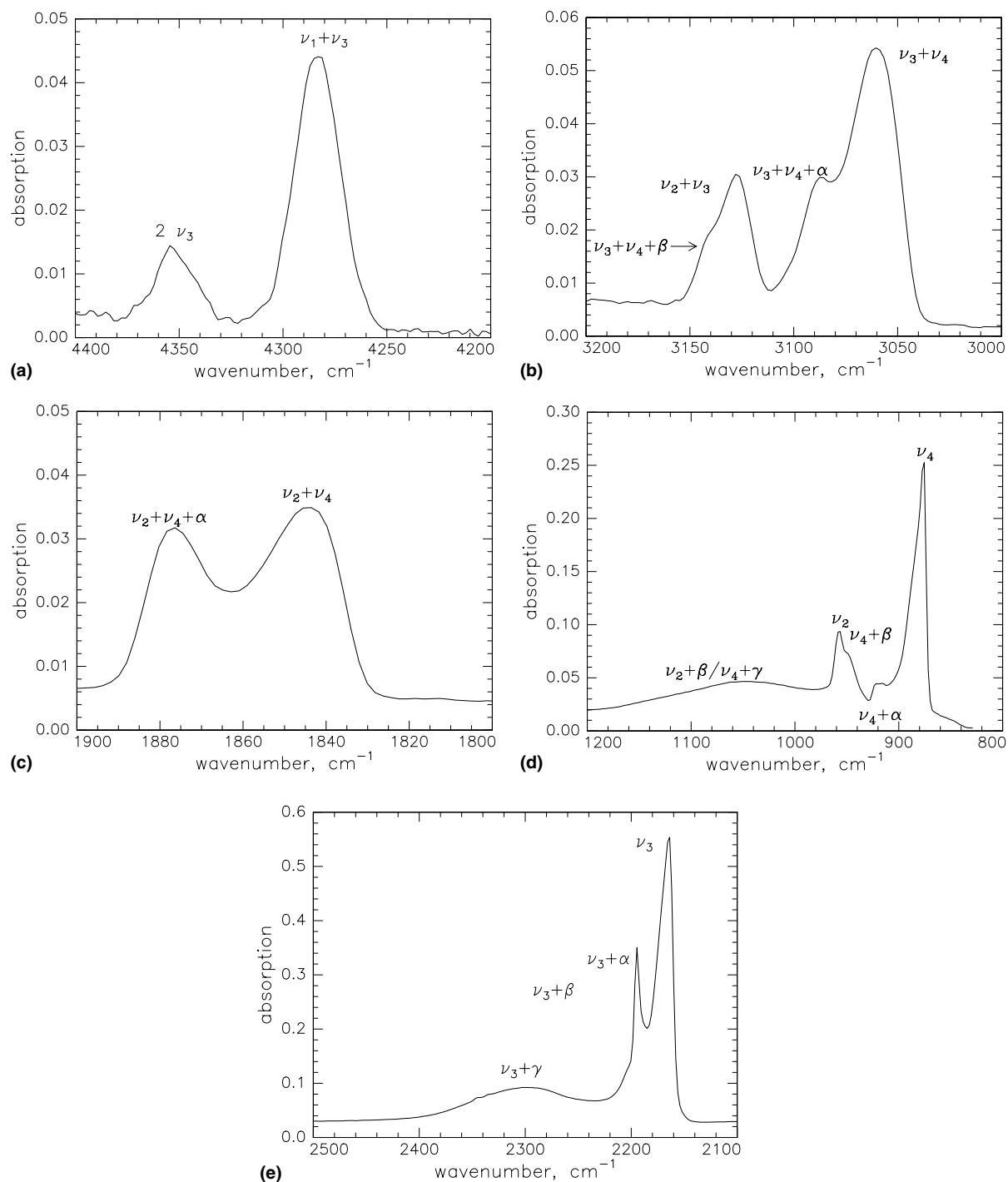


Fig. 2. Infrared spectrum of the silane frost at 10 K. The assignments of the peaks are compiled in Table 1. The insert shows the splitting of the $\nu_1 + \nu_3$ combination band at an elevated temperature of 59 K.

10, 100 and 1000 nA by scanning the electron beam over an area of $3.0 \pm 0.4 \text{ cm}^2$. Accounting for irradiation times of between 10 and 120 min and the extraction efficiency of 78.8% of the electrons, this exposes the targets from 3.0×10^{13} to 4.5×10^{16} electrons. To guarantee an identification of the reaction products in the ices and those subliming into the gas phase on line and in situ, a Fourier transform infrared spectrometer

(FTIR; solid state) and a quadrupole mass spectrometer (QMS; gas phase) were utilized. The Nicolet 510 DX FTIR spectrometer ($5000\text{--}500 \text{ cm}^{-1}$) operates in an absorption–reflection–absorption mode (reflection angle $\alpha = 75^\circ$) (resolution $0.5\text{--}2 \text{ cm}^{-1}$; spectra were averaged for 180 s). The infrared beam is coupled via a mirror flipper outside the spectrometer, passes through a differentially pumped potassium bromide (KBr) win-

Table 1

Infrared absorptions of the silane (left column) and d4-silane (center column) frosts (sh: shoulder); α , β , and γ denote lattice modes of the silane sample

Frequency (cm ⁻¹)	Frequency (cm ⁻¹)	Assignment
4354	3183	2 ν_3
4283	3128	$\nu_1 + \nu_3$
3142 (sh)	2264	$\nu_3 + \nu_4 + \beta$
3128	2243	$\nu_2 + \nu_3$
3087	2202	$\nu_3 + \nu_4 + \alpha$
3060	2173	$\nu_3 + \nu_4$
2300	1670	$\nu_3 + \gamma$
2250	1638	$\nu_3 + \beta$
2195	1607	$\nu_3 + \alpha$
2163	1581	ν_3
1876	1359	$\nu_2 + \nu_4 + \alpha$
1844	1334	$\nu_2 + \nu_4$
1050	781	$\nu_2 + \beta/\nu_4 + \gamma$
957	681	ν_2
948	703	$\nu_4 + \beta$
918	681	$\nu_4 + \alpha$
876	647	ν_4

dow, is attenuated in the ice sample prior and after reflection at a polished silver waver, and exits the main chamber through a second differentially pumped KBr window before being monitored via a liquid nitrogen cooled detector. The gas phase is monitored by a quadrupole mass spectrometer (Balzer QMG 420; 1–200 amu mass range) with electron impact ionization of the neutral molecules in the residual gas analyzer mode at electron energies of 100 eV and running the photomultiplier at 2000 V; dwell time of the masses were chosen to be 0.5 ms.

3. Theoretical approach

The molecular structures and vibrational frequencies of the disilyl and d5-disilyl radicals were examined in terms of ab initio molecular orbital methods. The geometries were optimized with the hybrid density functional B3LYP method, i.e. Becke's [25] three-parameter non-local exchange functional with the non-local correlation functional of Lee et al. [26] and the 6-311G(d,p) basis set [27]. Since the energy of the quartet electronic state of the Si₂H₅ species are extremely high and dissociative, we have only studied the doublet electronic state. We have examined various isomeric structures of Si₂H₅ species for mono-bridged, di-bridged, and tri-bridged geometries in addition to the H₃Si–SiH₂ structure. All optimized geometries with di-bridged and tri-bridged structures are shown to have more than two imaginary frequencies and they turned into either two structures when we optimized further along each imaginary mode. The vibrational frequencies and infrared intensities were obtained for optimized Si₂H₅ and its deuterated Si₂D₅

species. The coupled cluster CCSD(T) calculations [28,29] with the aug-cc-pVTZ basis set [30] were also performed at the optimized structures obtained with the B3LYP method in order to compare the relative energies for Si₂H₅ and C₂H₅ systems. All computations were carried out using the GAUSSIAN 98 program package [31]. The relative energies stated in the text are the values obtained with the CCSD(T) method corrected with the zero-point vibrational energies obtained with the B3LYP method.

4. Computational results

To identify the disilyl radical and its perdeuterated counterpart unambiguously, it is necessary to compute the infrared active absorptions frequencies of the Si₂H₅ and Si₂D₅ species and also to provide their integrated absorption coefficients of the normal modes. Fig. 3 illustrates the optimized structures of the Si₂H₅ species obtained with the B3LYP/6-311G(d,p) method; the energetics are compiled in Table 2. We have found only two energy minima which are denoted as **H3SiSiH2** and **HSiHSiH3**. The **H3SiSiH2** structure corresponds formally to the ethyl radical. It should be noted that the radical center of the SiH₂ moiety differs from the CH₂ part of ethyl radical being almost planar conformation. We would like to stress that a mono-bridged structure **H2SiHSiH2** is shown to be the transition state (TS) of a hydrogen shift between the two **H3SiSiH2** species. It is interesting that the SiH₂-moiety in this transition state bends out toward the same direction of shifting H atom. This structure substantially contrasts to the transition state of H-shift in ethyl radical as shown in Fig. 3. The reaction coordinate at the structure of **H2SiHSiH2** indicates that the SiH₂ groups have large amplitude in addition to the shifting hydrogen atom, while the hydrogen atom mainly moves at the H-shift TS of C₂H₅ radical. The energy of this transition state is calculated to be 118 kJ mol⁻¹ above **H3SiSiH2**; this energy is much lower than the energetics of the transition state of the corresponding hydrogen shift within the ethyl radical (168 kJ mol⁻¹).

The **HSiHSiH3** structure presents the second minimum; this isomer has already been shown by Wang and Huang [13]. The energy of this structure is 130 kJ mol⁻¹ higher than the global minimum **H3SiSiH2**; considering the geometry, this isomer can be described best as a hydrogen-bridged structure of a complex between a silane (SiH₄) and silylidyne (SiH) species. Wang and Huang [13] have shown that the **HSiHSiH3** isomer is a pre-complex of the insertion reaction of silylidyne into a silicon–hydrogen bond of a silane molecule; the intermediate formed isomerizes to the global minimum **H3SiSiH2**. We calculated the overall reaction energy to form **H3SiSiH2** from the separated reactants to be

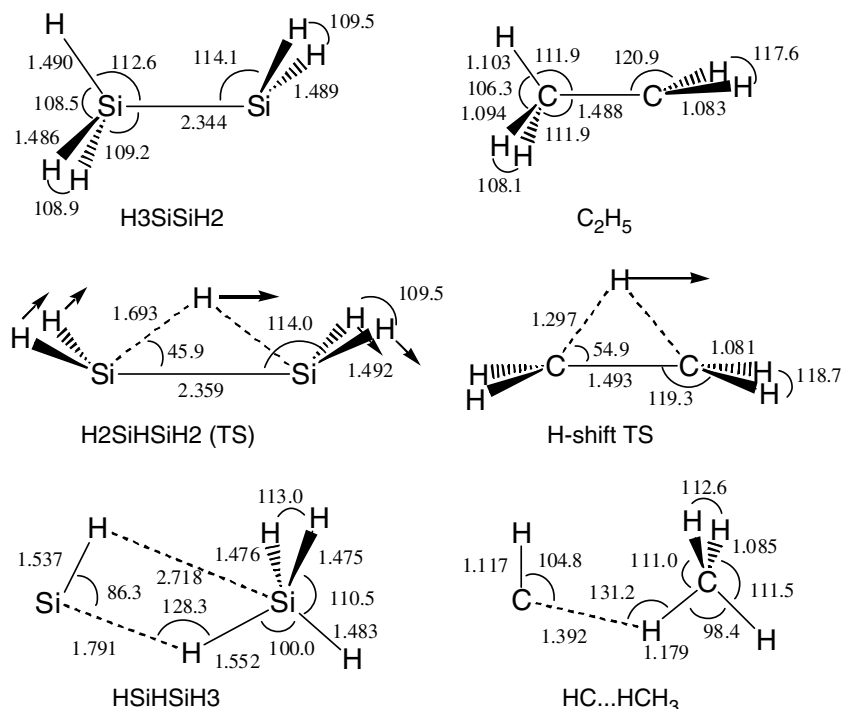


Fig. 3. Optimized structures of Si_2H_5 and C_2H_5 species calculated with the B3LYP/6-311G(d,p) method. The bond lengths and bond angles are given in units of Å and degrees, respectively. The arrows at the transition state structure indicate the direction of normal coordinate which has an imaginary frequency.

Table 2

Relative energies (kJ mol^{-1}) in the Si_2H_5 and C_2H_5 system evaluated with B3LYP/6-311G(d,p) and CCSD(T)/aug-cc-pVTZ at the geometries optimized with the B3LYP method

Si_2H_5	B3LYP	CCSD(T)	C_2H_5	B3LYP	CCSD(T)	Experimental
H_3SiSiH_2 (X^2A')	0	0	CH_3CH_2 (X^2A')	0	0	0
$\text{H}_2\text{SiHSiH}_2$ (TS)(X^2B_2)	117.8	121.3	H-shift TS(X^2B_2)	168.3	168.4	–
HSiHSiH_3 (X^2A)	132.6	130.3	HCHCH_3 (X^2A'')	379.6	378.4	–
SiH ($X^2\Pi$) + SiH_4 (X^1A_1)	154.9	163.2	CH ($X^2\Pi$) + CH_4 (X^1A_1)	393.6	383.8	400 ± 4
SiH_2 (X^1A_1) + SiH_3 (X^2A_1)	216.4	225.0	CH_2 (X^3B_1) + CH_3 (X^2A_2'')	402.1	398.9	413 ± 5

All energies are corrected with the zero point vibrational frequencies at the B3LYP level of calculation as given in Table 3.

only 33 kJ mol^{-1} which is slightly larger by 9 kJ mol^{-1} than the value obtained with the MP4 method [13]. The relative energies obtained in the present study are summarized in Table 2. The calculated vibrational frequencies and infrared intensities of the Si_2H_5 and Si_2D_5 species are compiled in Table 3. To estimate the accuracy of the energetics, we calculated also the C_2H_5 and C_2H_6 systems at the same levels of theory and compared these results to literature data (Tables 2 and 4) [32]. These data suggest that the calculations underestimate the reaction energies by $10\text{--}15 \text{ kJ mol}^{-1}$, i.e., the reactions are actually more endoergic than calculated.

To investigate the energetics of the proposed reaction sequence to form Si_2H_5 species via reactions (7)–(9), we computed also the energetics, vibrational frequencies, and the infrared intensities of the SiH_3 radical and of

both Si_2H_6 isomers (Figs. 4 and 5, Tables 4–6); these data are compared to the carbon analogous species. The molecular structure of silyl radical has C_{3v} symmetry which corresponds to sp^3 conformation in contrast to the planar sp^2 conformation of methyl radical. This structure difference reflects the vibrational frequency of umbrella motion (760 for SiH_3 and 506 cm^{-1} for CH_3).

5. Experimental results

Upon irradiation of the silane sample with an electron current of 10 nA at 10 K , absorptions of the silyl radical, $\text{SiH}_3(X^2A_1)$, appeared instantaneously at 722 cm^{-1} (Table 7, Fig. 5). The position of this ν_2 umbrella mode agrees well with previous studies utilizing hydro-

Table 3

Unscaled vibrational frequencies (cm^{-1}) and their infrared intensities (km mol^{-1}) of various Si_2H_5 and Si_2D_5 species calculated with B3LYP/6-311G(d,p) method

Symmetry	H3SiSiH2		Characterization	D3SiSiD2	
	Frequency (cm^{-1})	Intensity (km mol^{-1})		Frequency (cm^{-1})	Intensity (km mol^{-1})
C_s					
$\nu_1(\text{a}')$	2223	75	SiH ₃ asymmetric stretch	1600	56
$\nu_2(\text{a}')$	2199	72	Symmetric stretch	1571	15
$\nu_3(\text{a}')$	2188	101	Symmetric stretch	1564	70
$\nu_4(\text{a}')$	949	63	Umbrella	691	20
$\nu_5(\text{a}')$	936	2	Bending	676	16
$\nu_6(\text{a}')$	875	420	Umbrella	641	223
$\nu_7(\text{a}')$	596	18	Rocking	454	10
$\nu_8(\text{a}')$	424	3	Si–Si stretching	403	0
$\nu_9(\text{a}')$	405	20	Rocking	294	11
$\nu_{10}(\text{a}'')$	2231	158	SiH ₃ asymmetric stretching	1613	93
$\nu_{11}(\text{a}'')$	2213	48	SiH ₂ asymmetric stretching	1600	20
$\nu_{12}(\text{a}'')$	950	44	Deformation	680	23
$\nu_{13}(\text{a}'')$	637	1	Deformation	481	0
$\nu_{14}(\text{a}'')$	390	21	Deformation	278	10
$\nu_{15}(\text{a}'')$	127	0	Torsion	91	0
C_{2v}					
	H2SiHSiH2 (TS)			D2SiDSiD2 (TS)	
$\nu_1(\text{a}_1)$	2160	20	Symmetric stretch	1546	12
$\nu_2(\text{a}_1)$	1503	144	SiHSi bending	1083	75
$\nu_3(\text{a}_1)$	916	24	SiH ₂ bending	670	14
$\nu_4(\text{a}_1)$	676	14	SiH ₂ rocking	485	6
$\nu_5(\text{a}_1)$	400	0	Si–Si stretching	386	0
$\nu_6(\text{a}_2)$	2190	0	Asymmetric stretching	1585	0
$\nu_7(\text{a}_2)$	705	0	SiH ₂ rocking	516	0
$\nu_8(\text{a}_2)$	128	0	Deformation	93	0
$\nu_9(\text{b}_1)$	2205	211	Asymmetric stretching	1595	113
$\nu_{10}(\text{b}_1)$	904	26	SiHSi bending	643	13
$\nu_{11}(\text{b}_1)$	333	6	Rocking	235	3
$\nu_{12}(\text{b}_2)$	2161	226	Symmetric stretching	1545	125
$\nu_{13}(\text{b}_2)$	1240	41	Shifting motion of bridging H atom	879	23
$\nu_{14}(\text{b}_2)$	885	187	SiH ₂ bending	638	94
$\nu_{15}(\text{b}_2)$	225 <i>i</i>	17	Hydrogen shift	173 <i>i</i>	10
C₁					
	HSiHSiH3			DSiDSiD3	
$\nu_1(\text{a})$	2291	68	SiH ₃ asymmetric stretching	1658	43
$\nu_2(\text{a})$	2275	48	SiH ₃ asymmetric stretching	1639	40
$\nu_3(\text{a})$	2242	76	SiH ₃ symmetric stretching	1599	44
$\nu_4(\text{a})$	1988	252	HSi stretching	1430	128
$\nu_5(\text{a})$	1829	393	SiHSi stretching	1312	217
$\nu_6(\text{a})$	1209	56	SiHSi bending	863	30
$\nu_7(\text{a})$	957	59	SiH ₃ deformation	688	35
$\nu_8(\text{a})$	936	63	SiH ₃ deformation	673	35
$\nu_9(\text{a})$	887	341	SiH ₃ umbrella	654	168
$\nu_{10}(\text{a})$	754	39	HSiH ₃ deformation	546	20
$\nu_{11}(\text{a})$	648	99	HSi rocking	481	59
$\nu_{12}(\text{a})$	439	23	Rocking	322	11
$\nu_{13}(\text{a})$	234	0	Torsion	166	0
$\nu_{14}(\text{a})$	131	2	SiHSi bending	121	2
$\nu_{15}(\text{a})$	31	1	Torsion	22	1

gen, neon, argon, and krypton gas matrices (721–738 cm^{-1}) [33–35]. Note that a significantly weaker peak found at 702 cm^{-1} might be attributed to a different lattice site in the silane matrix. Both the ν_4 deformation (925–928 cm^{-1}) [33–35] and the ν_3 silicon–hydrogen stretching mode (2185 cm^{-1}) [36] remain unobservable

in our experiments because they are obscured by the fundamentals of the silane ice. An absorption at 820 cm^{-1} , which could be assigned to the ν_6 fundamental of the disilane molecule, $\text{Si}_2\text{H}_6(\text{X}^1\text{A}_{1g})$, also showed up immediately at the beginning of the irradiation (Fig. 5). Note that the less-intense deformation mode of the

Table 4

Relative energies (kJ mol⁻¹) of Si₂H₆ and C₂H₆ species and their fragments evaluated with B3LYP/6-311G(d,p) and CCSD(T)/aug-cc-pVTZ at the geometries optimized with the B3LYP method

Si ₂ H ₆	B3LYP	CCSD(T)	C ₂ H ₆	B3LYP	CCSD(T)	Experimental
H ₃ SiSiH ₃ (X ¹ A _{1g})	0	0	C ₂ H ₆ (X ¹ A _{1g})	0	0	0
H ₃ SiSiH ₃ (TS)(X ¹ A _{1'})	3.6	3.9	C ₂ H ₆ (TS)(X ¹ A _{1'})	10.2	10.5	
H ₂ SiHSiH ₃ (X ¹ A)	179.3	178.4	–	–	–	
SiH ₂ (X ¹ A ₁) + SiH ₄ (X ¹ A ₁)	205.0	213.7	CH ₂ (X ³ B ₁) + CH ₄ (X ¹ A ₁)	381.7	384.1	395
H(² S _{1/2}) + H ₃ SiSiH ₂ (X ² A')	358.5	359.8	H(² S _{1/2}) + C ₂ H ₅ (X ² A')	407.1	411.7	421
2 SiH ₃ (X ² A ₁)	287.6	304.7	2CH ₃ (X ² A ₂ ')	350.6	360.7	375

All energies are corrected with the zero point vibrational frequencies at the B3LYP level of calculation.

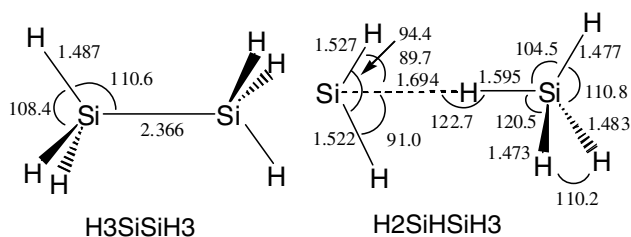


Fig. 4. Optimized structures of Si₂H₆ species calculated with the B3LYP/6-311G(d,p) method. The bond lengths and bond angles are given in units of Å and degrees, respectively.

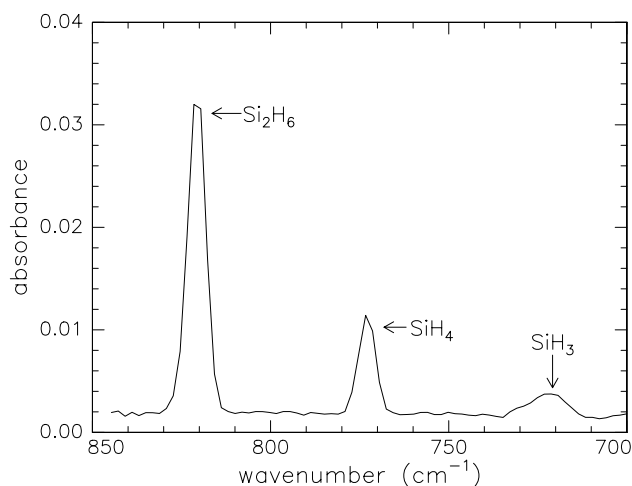


Fig. 5. New absorption features of the silyl radical, SiH₃(X²A₁), at 722 cm⁻¹ and of the disilane molecule, Si₂H₆(X¹A_{1g}), at 820 cm⁻¹ in the silane matrix at 10 K.

SiH₃ group is observable at 935 cm⁻¹ as a shoulder. The intensity ratio of the 820 versus the 935 cm⁻¹ band of about six agrees very well with the computed value (Table 5). The silicon–hydrogen stretching mode (2180–2152 cm⁻¹) remained unobservable since the fundamental overlaps with the absorption of the silane species. We were unable to detect absorptions of the SiH(X²Π) and SiH₂(X³A₁) species in the silane matrix. Likewise, the less stable H₂SiHSiH₃ isomer (Table 4, Fig. 4) remains elusive. We would like to stress that the assignments of all peaks was double checked in per-

deuterated silane (SiD₄) matrices. Here, we detected two fundamentals of the d₃-silyl radical, SiD₃(X²A₁), at 669 cm⁻¹ (ν₂; shoulder) and 540 cm⁻¹ (ν₄; Fig. 6); this assignment corresponds very well with previously assigned peak positions at 668 and about 546 cm⁻¹ in noble gas matrices. Likewise, the disilane molecule was observed in our experiments through its absorptions at 606 (ν₆; Fig. 6) and 1541 cm⁻¹ (ν₅; Fig. 7). Summarized, at low irradiation currents of 10 nA, solely absorptions of the silyl radical, SiH₃(X²A₁), and of the disilane molecule, Si₂H₆(X¹A_{1g}), together with their deuterated counterparts can be observed unambiguously in the silane matrix (Table 7).

After the actual irradiation experiments (10 nA), the samples were left isothermally at 10 K and then warmed up at a rate of 0.5 K min⁻¹. We observed a disappearance of the 702 and 722 cm⁻¹ bands at 45 ± 3 K. On the other hand, the intensity of the 820 and 935 cm⁻¹ absorptions do not decrease. This suggests that the silyl radical likely reacts – possibly barrier-less with atomic hydrogen – upon warming up the sample to 45 K. However, the reaction of thermalized hydrogen atoms – generated suprathemally via reaction (7) – with disilane via hydrogen abstraction involves an entrance barrier; since this barrier cannot be overcome at 40 K, we do not observe a degradation of the 820 and 935 cm⁻¹ peaks.

Having identified the silyl radical and the disilane molecule in low temperature silane matrices, we exposed the silane samples also to higher electron currents of 100 nA. The goal of this approach is to investigate if the disilane molecule can be degraded via Eq. (9) to form atomic hydrogen plus the disilyl radical, Si₂H₅(X²A'). Indeed, after irradiating the silane sample for 5 min at 100 nA, we were able to observe a new absorption at 843 cm⁻¹ in the silane matrix (Fig. 8) and at 621 cm⁻¹ in the perdeutero silane matrix (Fig. 9). We can compare now our calculated absorption frequencies with the experimentally observed ones. Accounting for a scaling factor of 0.97 – a reasonable value for the B3LYP/6-311G(d,p) level of theory – the theoretical data predict that the most intense absorption of the disilyl radical should be observable at 849 (Si₂H₅(X²A')) and 621 cm⁻¹ (Si₂D₅(X²A')); these predictions are in excellent agreement with our observations. Also, the blue shift

Table 5

Unscaled vibrational frequencies (cm^{-1}) and their infrared intensities (km mol^{-1}) of Si_2H_6 and Si_2D_6 species calculated with B3LYP/6-311G(d,p) method

H3SiSiH3			Characterization	D3SiSiD3	
	Frequency (cm^{-1})	Intensity (km mol^{-1})		Frequency (cm^{-1})	Intensity (km mol^{-1})
$\nu_1(\text{a}_{1g})$	2219	0	Symmetric stretch	1580	0
$\nu_2(\text{a}_{1g})$	927	0	Deformation	694	0
$\nu_3(\text{a}_{1g})$	421	0	Si-Si stretching	396	0
$\nu_4(\text{a}_{1u})$	135	0	Torsion	96	0
$\nu_5(\text{a}_{2u})$	2210	122	Symmetric stretch	1572	71
$\nu_6(\text{a}_{2u})$	854	546	Deformation	630	295
$\nu_7(\text{e}_g)$	2220	0	Stretching	1604	0
$\nu_8(\text{e}_g)$	945	0	Deformation	675	0
$\nu_9(\text{e}_g)$	636	0	Rocking	484	0
$\nu_{10}(\text{e}_u)$	2230	208	Stretching	1612	118
$\nu_{11}(\text{e}_u)$	960	92	Deformation	689	48
$\nu_{12}(\text{e}_u)$	381	27	Rocking	272	13
H2SiHSiH3			Characterization	D2SiDSiD3	
	Frequency (cm^{-1})	Intensity (km mol^{-1})		Frequency (cm^{-1})	Intensity (km mol^{-1})
$\nu_1(\text{a})$	2297	58	SiH_3 asymmetric stretching	1661	39
$\nu_2(\text{a})$	2273	64	SiH_3 asymmetric stretching	1639	45
$\nu_3(\text{a})$	2242	81	SiH_3 symmetric stretching	1599	43
$\nu_4(\text{a})$	2055	215	H_2Si asymmetric stretching	1479	117
$\nu_5(\text{a})$	2032	173	H_2Si symmetric stretching	1459	85
$\nu_6(\text{a})$	1674	185	SiHSi asymmetric stretching	1195	101
$\nu_7(\text{a})$	1297	9	SiHSi bending	933	6
$\nu_8(\text{a})$	990	42	H_2Si bending	711	27
$\nu_9(\text{a})$	960	41	SiH_3 deformation	692	45
$\nu_{10}(\text{a})$	957	73	SiH_3 deformation	685	13
$\nu_{11}(\text{a})$	914	64	HSiH_3 deformation	662	66
$\nu_{12}(\text{a})$	878	318	SiH_3 umbrella	638	128
$\nu_{13}(\text{a})$	661	112	H_2Si rocking	502	65
$\nu_{14}(\text{a})$	630	7	SiH_3 rocking	461	3
$\nu_{15}(\text{a})$	483	2	SiH_3 rocking	350	1
$\nu_{16}(\text{a})$	274	0	Torsion	196	0
$\nu_{17}(\text{a})$	152	2	Deformation	120	7
$\nu_{18}(\text{a})$	111	12	Deformation	92	5

Table 6

Unscaled vibrational frequencies (cm^{-1}) and their infrared intensities (km mol^{-1}) of the SiH_3 and SiD_3 radicals calculated with B3LYP/6-311G(d,p) method

SiH3			Characterization	SiD3	
	Frequency (cm^{-1})	Intensity (km mol^{-1})		Frequency (cm^{-1})	Intensity (km mol^{-1})
$\nu_1(\text{a}_1)$	2193	5	Symmetric stretch	1557	3
$\nu_2(\text{a}_1)$	760	77	Umbrella	561	84
$\nu_3(\text{e})$	2234	256	Asymmetric stretch	1616	144
$\nu_4(\text{e})$	973	132	Deformation	674	66

Table 7

Compilation of newly observed species and their absorptions in low temperature silane matrices

Species	Frequency (cm^{-1})	Fundamental	Frequency (cm^{-1})	Species
SiH_3	722	ν_2	540	SiD_3
	–	ν_4	669	
Si_2H_6	820	ν_6	606	Si_2D_6
	–	ν_5	1541	
	935	ν_8	–	
Si_2H_5	843	ν_6	621	Si_2D_5

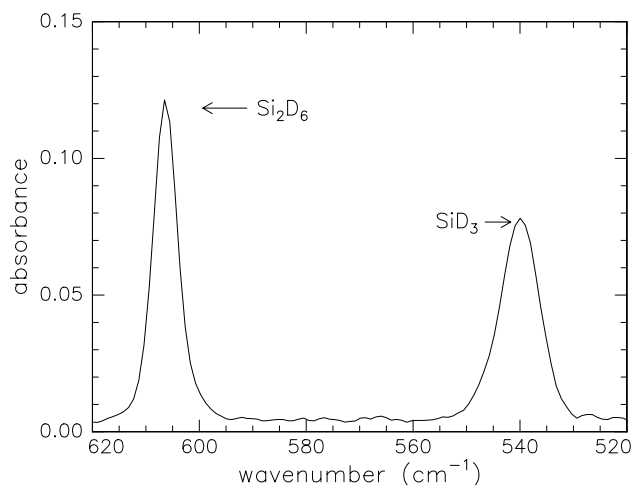


Fig. 6. New absorption features of the perdeutero silyl radical, $\text{SiD}_3(X^2A_1)$, at 540 cm^{-1} and of the perdeutero disilane molecule, $\text{Si}_2\text{D}_6(X^1A_{1g})$, at 606 cm^{-1} in the d4-silane matrix at 10 K.

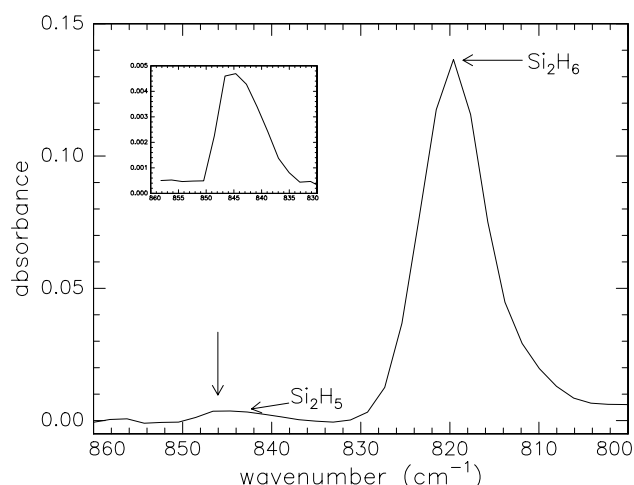


Fig. 8. New absorption features of the disilyl radical, $\text{Si}_2\text{H}_5(X^2A')$ at 844 cm^{-1} in silane at 10 K.

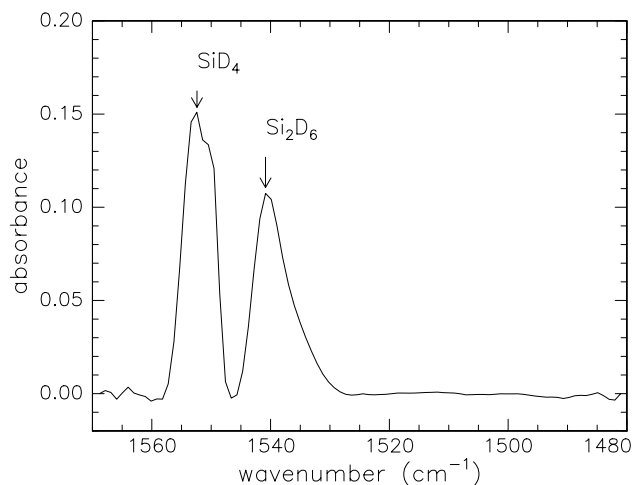


Fig. 7. New absorption features of the perdeutero disilane molecule, $\text{Si}_2\text{D}_6(X^1A_{1g})$, at 1541 cm^{-1} in the silane matrix at 10 K.

of the Si–H and Si–D deformation modes from 820 (Si_2H_6) to 844 cm^{-1} (Si_2H_5) and 606 (Si_2D_6) to 621 cm^{-1} (Si_2D_5) goes hand in hand with a change from a sp^3 to an sp^2 hybridized silicon atom. Note that the **HSiHSiH3** isomer was not observed. This suggests that the silicon–silicon bond of the disilane molecule is conserved during the electron-induced decomposition of disilane to form Si_2H_5 plus atomic hydrogen. We would like to stress that both peaks disappear upon warming the matrix to 35–40 K, whereas the absorptions of the disilane molecules do not change. This suggests that the new absorption feature comes from an open shell species which reacts upon annealing the matrix – similar to the silyl radical – possibly with mobile hydrogen atoms to ‘recycle’ disilane. For example, integrating the 621 and 844 cm^{-1} peaks and accounting for the infrared absorption coefficient suggest that about 10^{14} disilyl rad-

icals (and their deuterated counterparts) are synthesized per cm^2 sample area. At the same time, the silane matrix contains about 10^{16} disilane molecules per cm^2 . Therefore, even a quantitative conversion of disilyl radicals to disilane molecules in the warming-up phase of the sample leads only to an increase of about 1% in the column density of the silane molecules; this enhancement is not detectable with the experimental setup. Based on these considerations, we can conclude a positive identification of the disilyl and perdeutero disilyl radicals in low temperature silane matrices.

6. Discussion and summary

Our experimental data suggest that the response of the silane matrix upon the keV electron irradiation is dictated by a silicon–hydrogen single bond rupture which leads to the formation of atomic hydrogen and the silyl radical, $\text{SiH}_3(X^2A_1)$, Eq. (7). This mechanism is similar to the formation of silyl radicals in silane glow discharge processes [37,38]. However, it is important to note that each hydrogen atom requires an excess energy – the lattice binding energy – of a few tens of kJ mol^{-1} to escape from the initially formed $[\text{SiH}_3 \cdot \cdot \text{H}]$ matrix cage [39]; otherwise, the sole fate will be a recombination of atomic hydrogen with the silyl radical to recycle a silane molecule. Our mass spectrometric data support the formation of mobile hydrogen atoms in the silane matrix. Here, we see an increase of the ion current of $m/e=2$ (H_2 , silane matrix) and of $m/e=4$ (D_2 , d4-silane matrix); the temporal development of the hydrogen molecular ion is shown in Fig. 10. Since we were unable to identify any SiH_x or SiD_x species in the solid state, we can conclude that the molecular hydrogen is formed via recombination of two hydrogen atoms in the silane

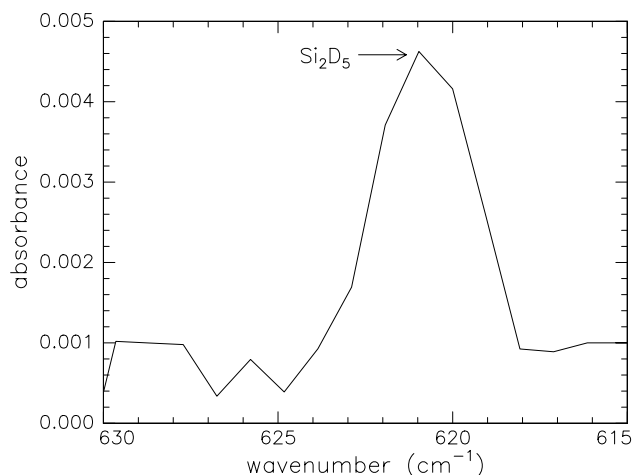
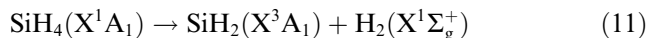
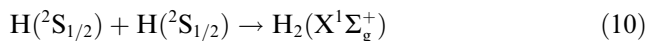


Fig. 9. New absorption features of the perdeutero disilyl radical, $\text{Si}_2\text{D}_5(\text{X}^2\text{A}')$ at 621 cm^{-1} in the d4-silane matrix at 10 K.

matrix (reaction (10)) rather than via reaction (11). We would like to stress that $m/e=2$ present the only signal detected with the mass spectrometer during the irradiation of the silane matrix at 10 K (Fig. 10). None of the SiH_x ($x=2-4$) species was found in the gas phase during the irradiation phase. This clearly demonstrates that $m/e=2$ is not a fragment from silicon hydride molecules in the gas phase. The mass spectrometric data also show that after the irradiation, the matrix stores thermalized hydrogen atoms; these atoms diffuse upon warming the matrix and recombine to molecular hydrogen. The latter is being released into the gas phase.



The infrared data suggest that the disilane molecule is formed initially within a single trajectory of the electron. It is important to note that in strong contrast to photons, each electron can release its kinetic energy via multiple energy transfers to various silane molecules. Utilizing the CASINO code [40], we find that each 5 keV electron loses 0.7 ± 0.1 keV of its kinetic energy while penetrating the silane target; this corresponds to an averaged electronic energy transfer of 3.3 ± 0.6 keV μm^{-1} . Since the dissociation energy of the Si–H bond has been determined to be 376 kJ mol^{-1} (3.89 eV) [41,42], we can conclude that each electron can generate up to 180 silyl radicals in the silane matrix. Considering the tetragonal unit cell of a silane crystal ($a_0=b_0=12.5\text{ \AA}$; $c_0=14.2\text{ \AA}$) which contains 32 silane molecules [23], each electron passes 156 ± 10 unit cells. Therefore, about one silyl radical is generated on average per unit cell. Here, *neighboring* silyl radical can recombine via Eq. (8) to form a disilane molecule $\text{Si}_2\text{H}_6(\text{X}^1\text{A}_{1g})$ inside the trajectory at 10 K. An alternative reaction, i.e., a diffusion-limited reaction mechanism of the silyl radical, can be safely ruled out: our infrared data suggest that at within the isothermal 10 K phase after the experiment, the signal of the silyl radical does not decrease. Therefore, we can conclude that the silyl radical is not mobile in 10 K silane matrix; this situation is very similar to the immobility of methyl radicals in 10 K methane matrices [39].

We attempt now to verify the postulated reaction mechanism to form the silyl radical and the disilane molecule energetically. As a typical example, we integrate

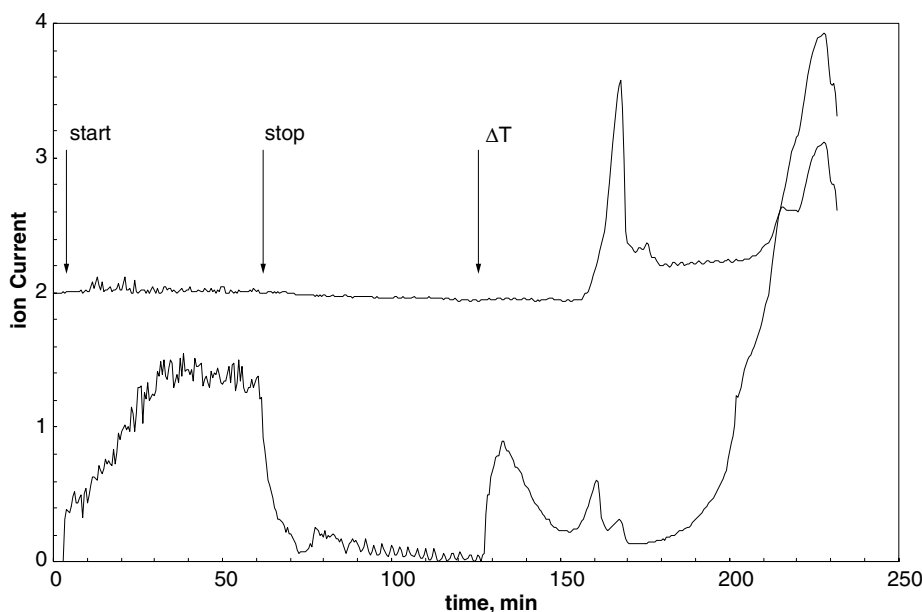


Fig. 10. Temporal profile of the silane ($m/e=32$; top) and molecular hydrogen ($m/e=2$; bottom) evolution during the irradiation (start–stop), the isothermal phase at 10 K, and the irradiation phase of the silane sample. ΔT indicates the onset of the annealing of the sample.

the absorptions of the silyl radical at 720 cm^{-1} and of the disilane molecule at 820 cm^{-1} 275 s after the start of the irradiation. Here, we find peak areas of 0.027 ± 0.002 and $0.147 \pm 0.002\text{ cm}^{-1}$, respectively. Accounting for the integral infrared absorption coefficients, the angle of reflection, and the surface area of the sample, 1.9 ± 0.4 silyl radicals and $1.5 \pm 0.2 \times 10^{15}$ disilane molecules. Therefore, $3.4 \pm 0.6 \times 10^{15}$ silicon–hydrogen bond ruptures in silane molecules are necessary. Accounting for the bond energy, this requires an energy of $1.3 \pm 0.2 \times 10^{16}$ eV. We can compare this value with the actual energy deposition. Irradiation (275 s) at 10 nA and 78.8% extraction efficiency of the electrons is equivalent to 1.4×10^{13} electrons penetrating the silane sample, i.e., an energy deposition of $9.5 \pm 1.4 \times 10^{15}$ eV. These data correlate very nicely with the energy deposition required to synthesize the spectroscopically observed silyl radicals and silane molecules; therefore we can conclude that reactions (7) and (8) are – within the error limits – the sole processes in 10 K silane matrices at low electron irradiation doses.

We like to address briefly the possibility of silicon atoms reacting with silane molecules to form Si_2H_4 isomers. Maier et al. [43] studied the interaction of silicon atoms with silane in low temperature matrices and concluded that silicon atoms can react in one step to form the disilyl molecule, $\text{H}_2\text{SiSiH}(\text{X}^2\text{A})$, via insertion. In our experiments, this process is unlikely. First, the reaction of free silicon atoms with hydrogen atoms in our silane matrix is expected to produce simple silicon hydrides such as SiH and SiH_2 through barrier-less recombination reactions. The infrared absorptions of these species are known [33] but could not be observed in our experiments. The silyl radical, $\text{SiH}_3(\text{X}^2\text{A}_1)$, is the only SiH_x ($x=1-3$) species which has been identified. The present data suggest also that this radical is formed instantaneously upon electron irradiation of the silane matrix simply because no absorptions of Si_2H_x ($x=1-6$) silicon bearing molecules appear at low irradiation times (Section 5). In addition, the new absorptions at 843 and 621 cm^{-1} , which we attributed to the $\text{Si}_2\text{H}_5(\text{X}^2\text{A}')$, and the d5-disilyl, $\text{Si}_2\text{D}_5(\text{X}^2\text{A}')$, radicals show up at longer irradiation exposure after the disilane molecules have been formed via recombination of silyl radicals. Most important however, we investigated the response of the silane matrix and the disilyl radicals toward even longer irradiation times [44]. Here, we saw – besides the peaks of the $\text{Si}_2\text{H}_5(\text{X}^2\text{A}')$, and the d5-disilyl, $\text{Si}_2\text{D}_5(\text{X}^2\text{A}')$, species – additional absorptions at 867 cm^{-1} (ν_5 ; H_3SiSiH), 635 cm^{-1} (ν_5 ; D_3SiSiD), 898 cm^{-1} (ν_{11} ; H_2SiSiH_2), and 658 cm^{-1} (ν_{11} ; D_2SiSiD_2). Based on the intensities of the bands, we can therefore discriminate between Si_2H_5 and Si_2H_4 isomers in the silane matrix.

Since the spectroscopic data indicate also a time-delayed production of the disilyl radical, $\text{Si}_2\text{H}_5(\text{X}^2\text{A}')$, it

is likely that overlapping cascades contribute to its formation via a silicon–hydrogen bond rupture in the initially formed disilane molecule through Eq. (9). Experiments in d4-silane matrices show a similar behavior, i.e., a deferred synthesis of d5-disilyl upon electron irradiation. Therefore, we can deduce that the disilyl radical is generated inside silane matrices via a three-step synthesis through reactions (7)–(9). The energy necessary to cleave the silicon–hydrogen bond was calculated to be about 360 kJ mol^{-1} . This is the very first time that an infrared absorption of the disilyl and d5-disilyl radical has been observed experimentally. The absorptions at 843 cm^{-1} ($\text{Si}_2\text{H}_5(\text{X}^2\text{A}')$) and 621 cm^{-1} ($\text{Si}_2\text{D}_5(\text{X}^2\text{A}')$) can now be utilized in future spectroscopic investigations of circumstellar envelopes of carbons stars and of CVD processes to follow the disilyl radical spectroscopically in real time rather than relying solely on mass spectrometric data as done previously.

Acknowledgements

The experiments were supported by the University of Hawai'i at Manoa (D.S. R.I.K.). The computations were carried out at the computer center of the Institute for Molecular Science, Japan, and supported by the Grants-in-Aid for Scientific Research on Priority Areas from the Ministry of Education, Science, and Culture, Japan (Y.O.).

References

- [1] T. Shirafuji et al., Jpn. J. Appl. Phys. 32 (1993) 1546.
- [2] J. Perrin, M. Shiratani, P. Kae-Nune, H. Videlot, J. Jolly, J. Guillon, J. Vac. Sci. Technol. 16 (1998) 278.
- [3] W. Kutzelnigg, Angew. Chem. Int. Ed. 23 (1984) 272.
- [4] M.B. Coolidge, D.A. Hrovat, W.T. Borden, J. Am. Chem. Soc. 114 (1992) 2354.
- [5] S.L. Girshickm, M.T. Swihart, S.M. Hu, M.R. Mahajan, S. Nijhawan, P. Electrochem. Soc. 98 (1999) 215.
- [6] M.T. Swihart, S.L. Girshick, J. Phys. Chem. B 103 (1999) 64.
- [7] P. Ho, M.E. Coltrin, J.S. Binkley, C.F. Melius, J. Phys. Chem. 90 (1986) 3399.
- [8] M.C. Ernst, A.F. Sax, J. Kalcher, Chem. Phys. Lett. 216 (1993) 189.
- [9] M.T. Swihart, J. Phys. Chem. A 104 (2000) 6083.
- [10] C. Pak, J.C. Rienstra-Kiracofe, H.F. Schaefer, J. Phys. Chem. A 104 (2000) 11232.
- [11] A. Matsuda, K. Tanaka, Thin Solid Films 92 (1982) 172.
- [12] B. Aka, E. Boch, J. Photoch. Photobio. A 150 (2002) 257.
- [13] Z.X. Wang, M.B. Haung, J. Chem. Soc., Faraday Trans. 94 (1998) 635.
- [14] S. Oikawa, M. Tsuda, S. Ohtsuka, J. Mol. Struct. 310 (1994) 287.
- [15] B. Ruscic, J. Berkowitz, J. Chem. Phys. 95 (1991) 2416.
- [16] B.E. Turner, Aatrophy. J. 376 (1991) 573.
- [17] R.I. Kaiser, Chem. Rev. 102 (2002) 1309.
- [18] D.M. Goldhaber, A.L. Betz, Astrophys. J. 279 (1984) L55.
- [19] C. Bennett, R. I. Kaiser, Monthly Notices Royal Astron. Society, submitted 2003.

- [20] C. Bennett, A. M. Mebel, R. I. Kaiser, *Phys. Chem. Chem. Phys.* submitted 2003.
- [21] W.M. Sears, J.A. Morrison, *J. Chem. Phys.* 62 (1975) 2736.
- [22] A. Nucara, P. Calvani, S. Lupi, P. Roy, *J. Chem. Phys.* 17 (1997) 6562.
- [23] P. Calvani, C. Ciotti, S. Cunsolo, S. Lupi, *Solid State Commun.* 75 (1990) 189.
- [24] R.P. Fournier et al., *Can. J. Chem.* 50 (1972) 35.
- [25] A.D. Becke, *J. Chem. Phys.* 98 (1993) 5648.
- [26] C. Lee, W. Yang, R.G. Parr, *Phys. Rev. B* 37 (1988) 785.
- [27] R. Krishnan, J.S. Binkley, R. Seeger, J.A. Pople, *J. Chem. Phys.* 72 (1980) 650.
- [28] J. Cizek, *Adv. Chem. Phys.* 14 (1969) 35.
- [29] J.A. Pople, M. Head-Gordon, K. Raghavachari, *J. Chem. Phys.* 87 (1987) 5968.
- [30] R.A. Kendall, T.H. Dunning, R.J. Harrison, *J. Chem. Phys.* 96 (1992) 6796.
- [31] M.J. Frisch et al., GAUSSIAN98, Revision A11, Gaussian Inc., Pittsburgh, PA, 2002.
- [32] Available from: <http://webbook.nist.gov/chemistry/>.
- [33] L. Andrews, X. Wang, *J. Phys. Chem. A* 106 (2002) 7696.
- [34] L. Li, J.T. Graham, W. Weltner, *J. Phys. Chem. A* 105 (2001) 11018.
- [35] N. Legay-Sommaire, F. Legay, *J. Phys. Chem. A* 102 (1998) 8759.
- [36] Y. Sumiyoshi, K. Tanaka, T. Tanaka, *Appl. Surf. Sci.* 79/80 (1994) 471.
- [37] L. Abouaf-Marguin, A. Lloret, *J. Non-Cryst. Solids* 77 & 78 (1985) 761.
- [38] A. Lloret, L. Abouaf-Marguin, *Chem. Phys.* 107 (1986) 139.
- [39] R.I. Kaiser, G. Eich, A. Gabrysch, K. Roessler, *Astrophys. J.* 484 (1997) 487.
- [40] D. Drouin, P. Hovington, R. Gauvin, *Scanning* 19 (1997) 1.
- [41] M.B. Coolidge, W.T. Bordon, *J. Am. Chem. Soc.* 110 (1988) 2298.
- [42] W. Thiel, A.A. Voityuk, *J. Mol. Struct. (Theochem.)* 313 (1994) 141.
- [43] G. Maier, H.P. Reisenauer, J. Glatthaar, *Chem. Eur. J.* 8 (2002) 4383.
- [44] D. S. Sillars, Y. Osamura, R. I. Kaiser, *Chem. Phys. Lett.* 2004, in press.